Pseudogap and Fermi surface in the presence of a spin-vortex checkerboard for 1/8-doped lanthanum cuprates

Pavel E. Dolgirev[1,2,*] and Boris V. Fine[1,3,†]

[1]*Skolkovo Institute of Science and Technology, Skolkovo Innovation Center, 3 Nobel Street, Moscow 143026, Russia*
[2]*Moscow Institute of Physics and Technology, 9 Institutskiy pereulok, Dolgoprudny, Moscow Region 141700, Russia*
[3]*Institute for Theoretical Physics, University of Heidelberg, Philosophenweg 12, 69120 Heidelberg, Germany*

(Received 23 May 2017; revised manuscript received 26 July 2017; published 17 August 2017)

The lanthanum family of high-temperature cuprate superconductors is known to exhibit both spin and charge electronic modulations around a doping level of 1/8. We assume that these modulations have the character of a two-dimensional spin-vortex checkerboard and investigate whether this assumption is consistent with the Fermi surface and the pseudogap measured by angle-resolved photoemission spectroscopy. We also explore the possibility of observing quantum oscillations of transport coefficients in such a background. These investigations are based on a model of noninteracting spin-1/2 fermions hopping on a square lattice and coupled through spins to a magnetic field imitating a spin-vortex checkerboard. The main results of this paper include (i) a calculation of the Fermi surface containing Fermi arcs at the positions in the Brillouin zone largely consistent with experiments, (ii) identification of factors complicating the observations of quantum oscillations in the presence of spin modulations, and (iii) an investigation of the symmetries of the resulting electronic energy bands, which, in particular, indicates that each band is doubly degenerate and has at least one conical point, where it touches another doubly degenerate band. We discuss possible implications these cones may have for the transport properties and the pseudogap.

DOI: 10.1103/PhysRevB.96.075137

I. INTRODUCTION

Several families of high-temperature cuprate superconductors are known to exhibit spin and/or charge modulations [1–11]. Resolving the character of these modulations acquired new urgency in recent decades in the context of efforts to reconcile angle-resolved photoemission spectroscopy (ARPES) experiments [12–15] with the measurements of quantum oscillations of various observables in response to magnetic field [16–21]. ARPES experiments in underdoped (hole-doped) cuprates generically observe open-ended lines of the Fermi surface known as Fermi arcs accompanied by an angle-dependent pseudogap. At the same time, observations of quantum oscillations indicate the presence of small closed Fermi surfaces. This phenomenology hinted at the possibility that Fermi arcs originate from closed Fermi surfaces in a smaller Brillouin zone (BZ) emerging as a result of some kind of periodically modulated background. Such interpretations based on one-dimensional stripelike or two-dimensional checkerboardlike charge modulations have, indeed, been proposed [22–28]. Spin modulations have mostly been omitted in these interpretations because of the absence of experimental evidence of the static spin response in $YBa_2Cu_3O_y$ (YBCO) and other cuprate families exhibiting quantum oscillations.

The cuprate family that does exhibit both spin and charge modulations is lanthanum cuprates. *A priori*, one may expect that the presence of spin modulations does not change the situation qualitatively, and hence, some sort of quantum oscillations would be present. Moreover, the experiments in Ref. [29] showed that one of the quantities exhibiting quantum oscillations in YBCO [17], namely, the Seebeck coefficient, exhibits the same overall trends in both $La_{1.8-x}Eu_{0.2}Sr_xCuO_4$ (Eu-LSCO) and YBCO as a function of both temperature and doping. Yet no experimental evidence of quantum oscillations has been reported so far for Eu-LSCO or other lanthanum cuprates. This may be due to the difficulty of producing sufficiently high quality samples, but there might also be deeper reasons.

The main focus of the present work is on 1/8-doped lanthanum cuprates, where elastic neutron scattering experiments [1] observed the fourfold splitting of the antiferromagnetic (π,π) peak and a later experiment [30] indicated that the modulation harmonics are linearly polarized in the direction transverse to the modulation wave vector. This leaves one with two possible interpretations, namely, (i) two domains of one-dimensional stripelike modulations or (ii) the two-dimensional checkerboard of spin vortices shown in Fig. 1. The above matter has been extensively discussed on the basis of both theoretical arguments and experimental evidence [31–37]. On the theoretical side, the situation was, in particular, analyzed on the basis of the Landau-type expansion in powers of the order parameter [37]. This analysis indicated that the ground states of both stripe and checkerboard patterns are possible, subject to material parameters, which are not known with the precision required to discriminate between the two possibilities. Microscopic models have also been investigated in this context (see, e.g., Refs. [38,39]), but here again, one can hardly rely on them because they either neglect or very crudely approximate quantitatively important factors such as medium-range Coulomb interaction and/or electron-lattice coupling. Various experiment-based arguments in favor of either stripes or checkerboards for lanthanum cuprates have been put forward in Refs. [31–37,40], but the issue has not been settled either. This issue is elusive not only in lanthanum cuprates but also for the yttrium-based and other cuprate families (see, e.g., Refs. [41–45]). Recently, a somewhat similar situation emerged in the context of the "spin-vortex crystal" proposal for iron-based superconductors [46–49].

*pavel.dolgirev@skolkovotech.ru
†b.fine@skoltech.ru

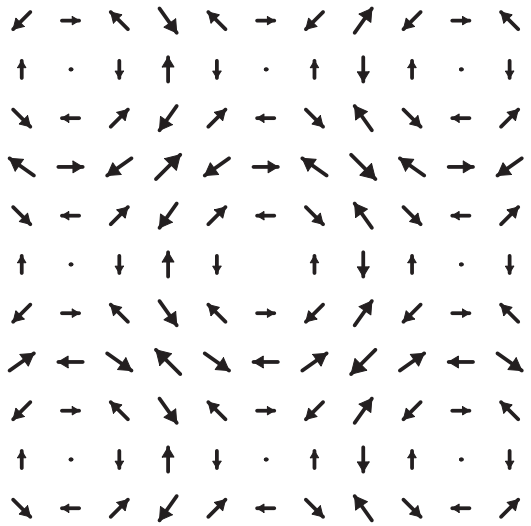

FIG. 1. Site-centered checkerboard corresponding to $\phi_1 = \phi_2 = 0$ in Eq. (3).

Fermi-surface reconstruction in the presence of stripelike spin and charge modulations was described theoretically in Ref. [25] in the context of ARPES experiments for 1/8-doped lanthanum cuprates. Here our goal is to study the Fermi surface properties assuming the presence of the spin-vortex checkerboard shown in Fig. 1. We develop a model of noninteracting fermions of spin 1/2 on a square lattice coupled through spins to local fields that mimic such a checkerboard. These local fields originate from the exchange interaction, which, in turn, has its origin in the interplay of the Coulomb interaction and the kinetic energy of electrons. Therefore, in leading order, the relativistic orbital effects of this local field can be neglected.

Our main results include (i) the reproduction of Fermi arcs at the positions observed experimentally, (ii) the identification of factors complicating the observations of quantum oscillations in the presence of spin modulations, and (iii) the discovery that the model has a symmetry forcing each energy band to have at least one point where it forms a conical connection to another band of the kind well known from the physics of graphene [50]. Such a property may drastically influence transport properties of the system. Moreover, this ubiquitous presence of conical points is a potential origin of the pseudogap. We also consider another scenario for the emergence of the pseudogap, which turned out to be more likely for the model parameters estimated to be relevant to lanthanum cuprates.

This paper is organized as follows: In Sec. II, we formulate our model and discuss its relevance to 1/8-doped lanthanum cuprates. In Sec. III, we investigate symmetries of the model and show that energy bands necessarily exhibit cones. In Sec. IV, we propose two scenarios for the emergence of the pseudogap and in Sec. V perform a calculation for a particular set of model parameters relevant to 1/8-doped lanthanum cuprates, thereby illustrating how our model can describe the pseudogap and the Fermi arcs. In Sec. VI, we discuss various parameter regimes and possible generalizations of the model and also place our results in the context of broader experimental knowledge about electronic transport in 1/8-doped lanthanum cuprates, addressing, in particular, the possibility to observe quantum oscillations. Finally, the main conclusions are summarized in Sec. VII.

II. MODEL

We consider a model of noninteracting spin-1/2 fermions on a square lattice in the background of 8×8 periodic modulation of local fields as in Fig. 1. The Hamiltonian is as follows:

$$\mathcal{H} = \mathcal{H}_0 + \sum_{i,j;\alpha,\beta} a^\dagger_{ij,\alpha}\left(B^x_{ij} S^x_{\alpha,\beta} + B^y_{ij} S^y_{\alpha,\beta}\right) a_{ij,\beta}, \qquad (1)$$

where i,j are the lattice indices, α,β are the indices of spin polarizations $\pm 1/2$ along the z axis, $a_{ij,\alpha}$ are the fermionic annihilation operators, $S^x_{\alpha,\beta}$, $S^y_{\alpha,\beta}$ are the spin-1/2 operators, and $\mathcal{H}_0$ is the tight-binding Hamiltonian with hopping to the first, second, and third nearest neighbors, which has the following spectrum

$$E_0(\mathbf{k}) = 2t(\cos k_x + \cos k_y) + 4t' \cos k_x \cos k_y + 2t''(\cos 2k_x + \cos 2k_y). \qquad (2)$$

The local fields $\mathbf{B}_{ij}$ depend on the lattice site positions as follows:

$$\mathbf{B}_{i,j} = (-1)^{i+j}\left[\begin{pmatrix} B_0 \\ 0 \end{pmatrix} \cos\left(\frac{\pi}{4} j + \phi_1\right) + \begin{pmatrix} 0 \\ B_0 \end{pmatrix} \cos\left(\frac{\pi}{4} i + \phi_2\right)\right], \qquad (3)$$

where ϕ_1 and ϕ_2 are two fixed phases of the two orthogonal harmonics. For Fig. 1, $\phi_1 = \phi_2 = 0$, but we would like to consider the general case.

As the fermions fill one-particle states of the Hamiltonian $\mathcal{H}$, the system exhibits the 8×8 modulation of spin polarizations that follow the local magnetic field. It is accompanied by 4×4 checkerboard modulation of the particle density of the form $n_{i,j} = n_0 + \delta n_{i,j}$, with $\delta n_{i,j} \propto |\mathbf{B}_{i,j}|^2$. Such spin- and charge-density modulations are consistent with the experiments [1]. This is therefore the minimal model describing the low-energy spin checkerboard response possibly emerging as a result of the delicate balance between large contributions from kinetic energy, Coulomb energy (including spin exchange), and the electron-lattice interaction.

Details of the numerical solution

We obtain the density of states (DOS) $\nu(E)$ and other quantities of interest by directly diagonalizing Hamiltonian $\mathcal{H}$ in Eq. (1). The diagonalization is done in the basis of the Bloch eigenstates of the Hamiltonian $\mathcal{H}_0$: $\{|\mathbf{k},\pm\rangle\}$, where the $+$ or $-$ represents the projection of the particle's spin on the z axis and $\mathbf{k} \equiv (k_x,k_y)$ is a wave vector belonging to the first BZ of the square lattice: $-\pi \leqslant k_x,k_y < \pi$. We refer to it as the "large BZ."

The 8×8 modulation of the local field reduces the BZ to $-\pi/8 \leqslant k_x,k_y < \pi/8$ ("small BZ"). The modulated terms in the Hamiltonian couple only those basis states in the large BZ which, after backfolding to the small BZ, have the same $\tilde{\mathbf{k}}$. These wave vectors are $\mathbf{k}_{l,m} = \tilde{\mathbf{k}} + \frac{\pi}{4} l \mathbf{e}_x + \frac{\pi}{4} m \mathbf{e}_y$, where

$\mathbf{e}_x \equiv (1,0)$, $\mathbf{e}_y \equiv (0,1)$, and $l,m = 0,\ldots,7$. Taking into account the fact that, for each of the 64 thus defined wave vectors, there are also two spin states coupled by the local-field terms, we obtain the energy spectrum for each $\tilde{\mathbf{k}}$ by diagonalizing the 128×128 Hamiltonian matrix, which has the following structure:

(1) $\langle \mathbf{k}_{l,m}, \pm | \mathcal{H} | \mathbf{k}_{l,m}, \pm \rangle = E_0(\mathbf{k}_{l,m})$.

(2) $\langle \mathbf{k}_{l_1,m_1}, + | \mathcal{H} | \mathbf{k}_{l_2,m_2}, - \rangle = \frac{i}{4} B_0 e^{\pm i\phi_2}$ for $(l_2 - l_1 \pm 1)[\mathrm{mod}\, 8] = 4$ and $(m_2 - m_1)[\mathrm{mod}\, 8] = 4$.

(3) $\langle \mathbf{k}_{l_1,m_1}, + | \mathcal{H} | \mathbf{k}_{l_2,m_2}, - \rangle = \frac{1}{4} B_0 e^{\pm i\phi_1}$ for $(m_2 - m_1 \pm 1)[\mathrm{mod}\, 8] = 4$ and $(l_2 - l_1)[\mathrm{mod}\, 8] = 4$.

Elsewhere, matrix elements are equal to zero.

III. SYMMETRIES AND DEGENERACIES OF ENERGY BANDS

A. Double degeneracy of energy bands

Here we show that each energy band in the spin-vortex checkerboard model is at least twice degenerate.

Let $\hat{T}_x$ be an operator representing translation by four lattice periods along the x direction and subsequent rotation of spins through 180° about the x axis. Analogously, let $\hat{T}_y$ be an operator representing translation by four lattice periods along the y direction and subsequent rotation of spins through 180° about the y axis. These operators have the following representation:

$$\hat{T}_x \equiv \hat{\tau}_{(4,0)} \otimes (i\sigma_x), \tag{4}$$

$$\hat{T}_y \equiv \hat{\tau}_{(0,4)} \otimes (i\sigma_y), \tag{5}$$

where σ_α are the Pauli matrices and $\hat{\tau}_{\mathbf{a}}$ is the translation by vector $\mathbf{a}$.

We now observe that operators $\hat{T}_x$ and $\hat{T}_y$ commute with the Hamiltonian but do not commute with each other, and in addition, they do not change wave vector $\mathbf{k}$. Therefore, each energy level for any given wave vector $\mathbf{k}$ is at least twice degenerate, which means that each energy band is at least doubly degenerate.

B. Conical touch points

We now show that at $\mathbf{k}_0 = (\frac{\pi}{8}, \frac{\pi}{8})$ each energy level is four times degenerate. This wave vector is a special high-symmetry point, because it is at the corner of the small BZ, and therefore, all symmetry transformations map it either into itself or into three other wave vectors, $(-\frac{\pi}{8}, \frac{\pi}{8})$, $(\frac{\pi}{8}, -\frac{\pi}{8})$, or $(-\frac{\pi}{8}, -\frac{\pi}{8})$, all of which are equivalent in the sense that they are connected by vectors of the reciprocal lattice. Although Hamiltonian (1) is not time reversal invariant, it is symmetric with respect to transformation $\hat{\tau}_{(4,4)}\mathcal{T}$, where $\mathcal{T}$ is the time-reversal operator. Importantly, the operator $\hat{\tau}_{(4,4)}\mathcal{T}$ transforms the wave vector $\mathbf{k}_0 = (\frac{\pi}{8}, \frac{\pi}{8})$ into an equivalent wave vector $(-\frac{\pi}{8}, -\frac{\pi}{8})$. As shown in Appendix A, this leads to the desired fourfold degeneracy.

The above proof implies that, at the wave vector $\mathbf{k}_0 = (\frac{\pi}{8}, \frac{\pi}{8})$, one doubly degenerate energy band touches another doubly degenerate energy band, which generally leads to a linear spectrum near the touching point; that is, the touching energy bands have a conical shape near $\mathbf{k}_0$ (see Figs. 4 and 5 below).

We also can generalize our Hamiltonian by including additional terms, such as the ones that induce charge-density modulations and/or superconductivity. Cones are robust to any such terms, provided they commute with $\hat{T}_x$, $\hat{T}_y$, and $\hat{\tau}_{(4,4)}\mathcal{T}$. One such obvious example is a potential proportional to $|\vec{B}_{i,j}|^2$ acting on charge density.

C. Plaquette-centered checkerboard

The case $\phi_1 = \phi_2 = \frac{\pi}{8}$ in Eq. (3) corresponds to the plaquette-centered checkerboard shown in Fig. 8. This lattice possesses unique symmetries, and as we show in Appendix B, these symmetries result in eightfold degeneracy of each energy level at the wave vector $\mathbf{k}_0 = (\frac{\pi}{8}, \frac{\pi}{8})$.

IV. TWO SCENARIOS OF PSEUDOGAP

We assume that, in real materials, the pseudogap in the one-particle density of states $\nu(E)$ around the Fermi energy E_F arises from the same energy balance that simultaneously determines the amplitude of the spin modulation. Therefore, in terms of the model description, we first obtain $\nu(E)$ for fixed values of t, t', t'', and B_0, then identify a dip associated with the pseudogap, and then choose the concentration of fermions such that E_F corresponds to the minimum of that dip.

We consider two scenarios for the origin of the pseudogap: the "conical-point scenario" and "band-edge scenario."

A. Conical-point scenario

In Sec. III, we showed that there are cones in the electronic energy spectrum; therefore, one would expect $\nu(E)$ to be suppressed near these conical touch points, and thus, the emergence of the pseudogap is associated with the chemical potential being pinned at one of these points. For the parameters choice relevant to lanthanum cuprates, cones are not likely to be isolated in the sense that, at such a chemical potential, there are additional contributions from regular Fermi surface pockets. This would make the conical-point scenario not very different from the more general band-edge scenario described below. Yet, as discussed in Sec. VI, the isolated conical-point scenario might be realized if additional terms are included in the model Hamiltonian.

B. Band-edge scenario

In general, the checkerboard modulation does not lead to clear energy gaps between the energy bands. As the modulation amplitude B_0 increases, some of the energy bands develop a clear gap between themselves, while other bands still have states within that gap. This results in an incomplete suppression of the density of states, which we associate with the band-edge scenario. Section V illustrates this scenario on the basis of a concrete calculation.

V. CALCULATIONS FOR A BAND-EDGE SCENARIO

A. Choice of parameters and density of states

Here we focus on the site-centered case $\phi_1 = \phi_2 = 0$ (see Fig. 1). Below, following Ref. [51], we fix $t = -1$, $t' = -0.17t$, and $t'' = -0.5t'$. For comparison with experiments,

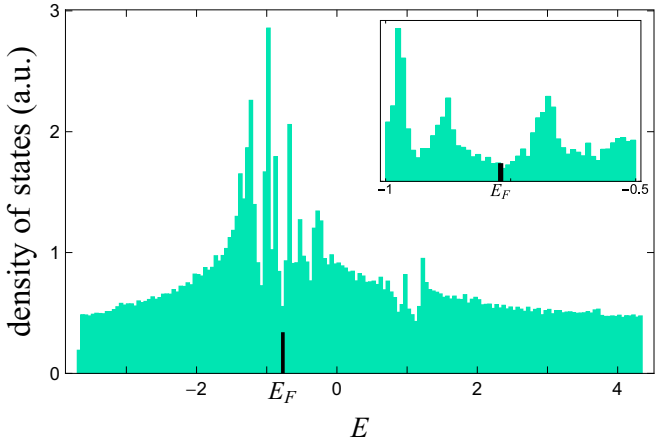

FIG. 2. Density of states in our model for $t = -1, t' = 0.17, t'' = -0.5t'$, and $B_0 = 0.5$. The black bar indicates the minimum of the DOS. The inset zooms in on the region close to the dip.

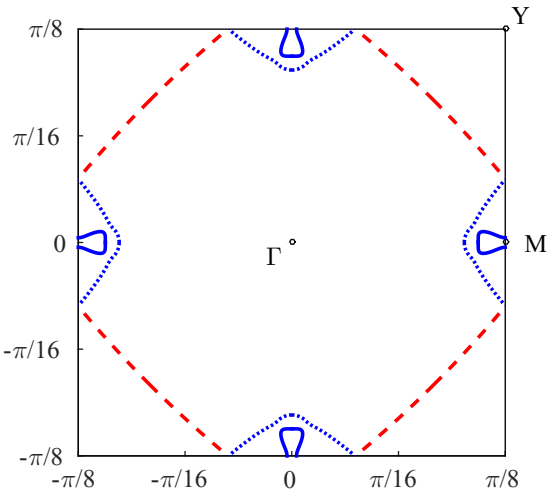

FIG. 3. Calculated Fermi surface in the small BZ. It consists of three disjoint pockets: the largest pocket, represented by the dashed red line, is electronlike; the two smaller pockets, represented by the dotted blue line and solid blue line, are holelike. The two larger pockets (electronlike and dotted holelike) almost touch, thereby nearly forming a joint Fermi surface that has the character of a connected network in momentum space.

energy unit 1 corresponds to approximately 350 meV. We use the local field amplitude $B_0 = 0.5$.

The density of states $\nu(E)$ for the above choice of parameters is shown in Fig. 2. Following the approach outlined in Sec. IV, we place the Fermi level at $E_F = -0.77$, which, as shown in Fig. 2, is located at the deepest minimum in $\nu(E)$ in the energy range approximately expected to correspond to the hole-doping level $1/8$. We identify this dip with the pseudogap. Such a choice leads to the concentration of fermions equal to 0.849 per site, which is reasonably close to the value of 0.875 expected for $1/8$-doped lanthanum cuprates. The discrepancy here is not of significant concern since the concentration depends on the properties of the model far from the Fermi level, where the model is not supposed to be quantitatively accurate. We have numerically computed the amplitude of the spin modulation, associated with the above concentration, to be equal approximately $0.3 \times 1/2$, which is consistent with the spin modulation amplitude reported by muon-spin relaxation (μSR) experiments [52]. This justifies our choice of the magnetic field amplitude B_0.

We further note that spin superstructure necessarily leads to charge-density modulation $\delta n_{i,j}$ proportional to $|\mathbf{B}_{i,j}|^2$. The amplitude of this modulation obtained numerically is approximately 2%.

B. Fermi surface in the small Brillouin zone

Next, we obtain the Fermi surface in the small BZ. It is shown in Fig. 3. The Fermi surface consists of three disjoint parts: a large electron pocket (with area equal to ∼0.4% of the total area of the large BZ) and two small hole pockets (the larger of them is ∼0.05% of the area of the large BZ). Figure 3 may convey the incorrect impression that the electron pocket and the larger hole pocket touch each other and, therefore, the Fermi surface forms a connected network in the k space. In Fig. 4 we demonstrate that the electron pocket and hole pockets are actually disjoint. They originate from different bands. Interestingly, all three bands in Fig. 4, which contribute to the Fermi surface, originate from the same cone at the Y point [$Y = (\frac{\pi}{8}, \frac{\pi}{8})$]. The cone for one of the bands (dashed red line in Figs. 3 and 4) is further illustrated in Fig. 5.

Figure 4 shows that five bands come close to the Fermi level: three of them contribute to the Fermi surface, while the remaining two are repelled just around E_F. That is why we call this scenario band edge.

C. Fermi surface in the large Brillouin zone

Let us specify the procedure of mapping the states from the small BZ to the large BZ. As described in Sec. II, each eigenstate associated with a wave vector in the small BZ is represented by a superposition of initial states (eigenstates of the tight-binding Hamiltonian $\mathcal{H}_0$) that correspond to wave vectors in the large BZ:

$$|\tilde{\mathbf{q}}\rangle = \sum_{l,m=0,\ldots,7;\alpha=\pm} C_{lm,\alpha} \left| \tilde{\mathbf{q}} + \frac{\pi}{4} l \mathbf{e}_x + \frac{\pi}{4} m \mathbf{e}_y, \alpha \right\rangle. \quad (6)$$

This gives the mapping from the small BZ to the large one: the sum $|C_{lm,+}|^2 + |C_{lm,-}|^2$ represents the spectral weight at the wave vector $\tilde{\mathbf{q}} + \frac{\pi}{4} l \mathbf{e}_x + \frac{\pi}{4} m \mathbf{e}_y$ in the large BZ.

In order to obtain the Fermi surface in the large BZ, we have chosen a sufficiently fine grid of wave vectors $\tilde{\mathbf{q}}$ in the small BZ. For each $\tilde{\mathbf{q}}$, we numerically computed the eigenstates in Eq. (6), then selected those that fell in the energy window $E = -0.77 \pm 0.03$, and then, for each one, plotted the spectral weights of the participating wave vectors $\tilde{\mathbf{q}} + \frac{\pi}{4} l \mathbf{e}_x + \frac{\pi}{4} m \mathbf{e}_y$. The result of such a mapping is shown in Fig. 6. In Appendix C, we further illustrate contributions in the large BZ from each of the three Fermi surface pockets present in the small BZ.

In Fig. 6, one can clearly see Fermi arcs in the nodal directions. Other spots of lower intensity also appear, but so far, they have not been observed in experiments. A comparison of Figs. 6 and 9 indicates that the Fermi arcs originate from

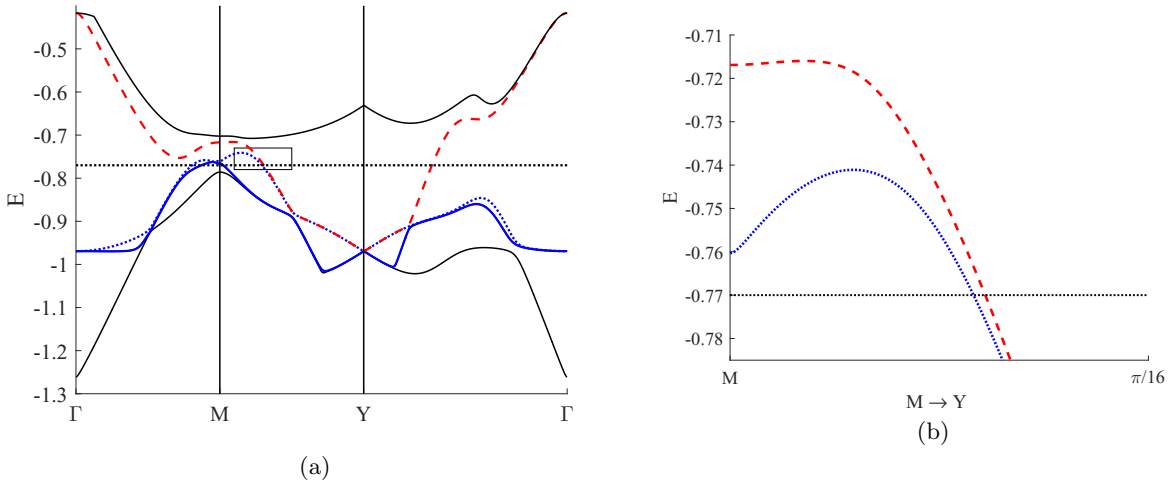

FIG. 4. (a) Cuts of energy bands in the small BZ close to the Fermi level (horizontal line). The Fermi surface originates from three bands; nevertheless, the contribution from one of the bands is relatively small (compare with Fig. 3). All three bands originate from the same cone at the Y point. (b) Close-up of the region in the rectangle in (a). We see that, indeed, the largest hole pocket and the electron pocket arise from different bands.

the largest Fermi surface pocket in the small BZ, while the remaining spots originate from the two smaller pockets. These smaller pockets are likely related to the noninteracting character of our model. They may possibly be removed if superconducting fluctuations are introduced (see Ref. [28]).

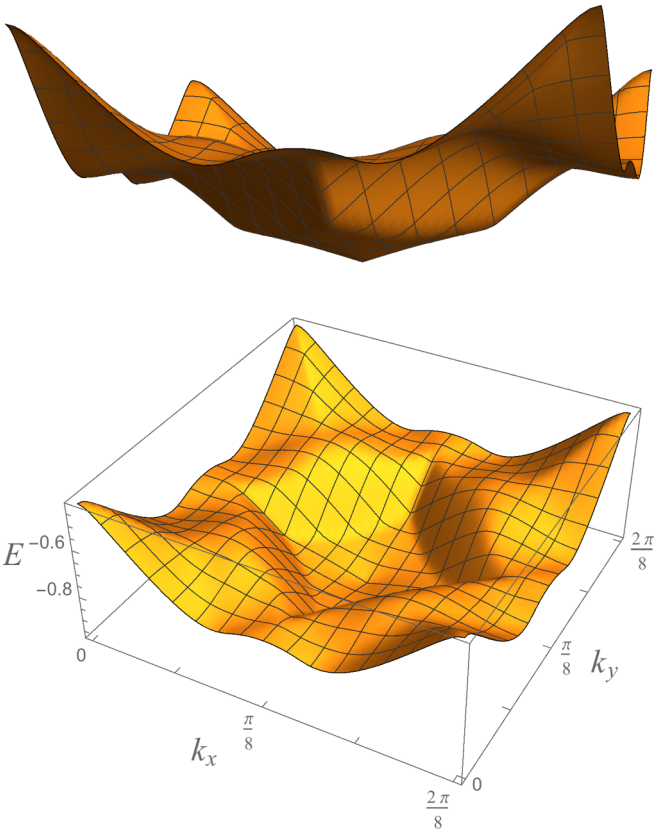

FIG. 5. Different views of the 3D band corresponding to the red dashed line in Figs. 3 and 4. The top illustration shows the cone at $\mathbf{k}_0 = (\frac{\pi}{8}, \frac{\pi}{8})$.

VI. DISCUSSION

Let us first consider the isolated conical-point scenario described in Sec. IV. It requires either a large value of the local-field amplitude B_0 or the inclusion of extra terms in the Hamiltonian not considered in the present paper, such as those associated with charge-density and lattice modulations [53] and/or superconducting fluctuations [28], provided these terms would respect the symmetries discussed in Sec. III. They may further separate energy bands and, as a result, isolate cones. In real materials, contributions from such terms might be large, and hence, the isolated conical-point scenario would become relevant. If this scenario is realized, then it would lead to the absence of quantum oscillations, because, in such a case, the

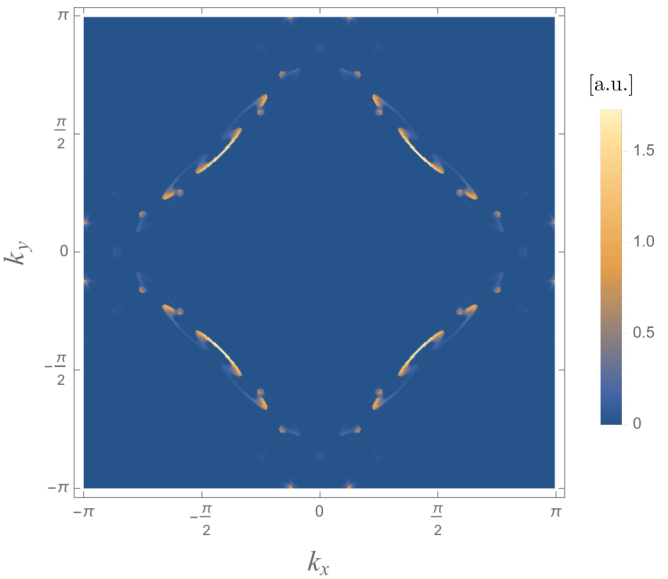

FIG. 6. Reconstructed Fermi surface in the large BZ. The procedure for its reconstruction is specified in the text.

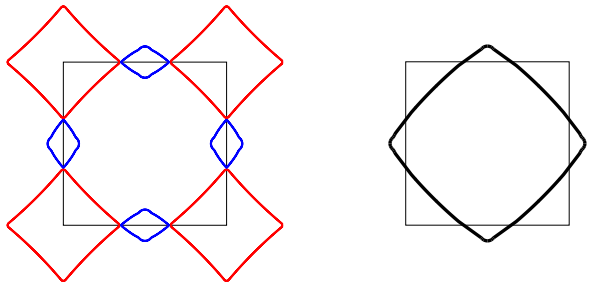

FIG. 7. (a) Quantum oscillations at low magnetic field $H \ll H_c$ contain contributions from both the electron pocket depicted by the dashed red line and the larger hole pocket depicted by the dotted blue line (compare with Fig. 3). (b) At large magnetic field $H \gg H_c$, semiclassical wave packets on the Fermi surface move as if the two pockets in (a) merge into a single Fermi surface depicted by the solid black line.

Fermi surface in the small BZ would be reduced to a single point.

The band-edge scenario leads to parameter-dependent predictions. Let us first analyse the example computed in Sec. V. The Fermi surface in Fig. 3 contains two pockets which, at the BZ boundary, almost touch each other. (Here we neglect the smallest Fermi surface pocket.) This suggests the possibility of magnetic breakdown between the corresponding bands. We estimate the characteristic field H_c for the onset of magnetic breakdown from the condition [54] $\frac{e\hbar H_c}{mc} \sim \frac{\epsilon_g^2}{W}$, where $W \sim 0.3t$ is the characteristic bandwidth [see Fig. 4(a)] and ϵ_g is a gap at E_F between the two bands. As one can see in Fig. 4(b), $\epsilon_g \lesssim 0.03t$, resulting in $H_c \lesssim 10$ T. Figure 7(a) illustrates electron and hole pockets contributing to quantum oscillations at low magnetic field $H \ll H_c$. Due to the smallness of each pocket, observations of quantum oscillations would probably require samples with an unrealistically long quasiparticle lifetime. In the opposite limit $H \gg H_c$, semiclassical fermionic wave packets will follow the trajectory in the momentum space shown in Fig. 7(b). This trajectory switches between the available Fermi surface pockets. The resulting pocket is holelike, with a total area of $\sim$1.3% of the large BZ, large enough to be detectable.

We now draw general lessons from the above example. The spin-vortex checkerboard modulation in the interesting range of parameters produces quite a dense set of energy bands with many symmetries. It is therefore to be expected that these bands have quite a few avoided crossings, which, in turn, if sliced at constant energy, would lead to multiple Fermi surfaces nearly touching each other. Such a pattern of Fermi surfaces is likely to suppress quantum oscillations because of multiple points where, at moderate external magnetic fields, magnetic breakdowns may occur, so that, effectively, the Fermi surface is turned into an open network in the momentum space without a well-defined cyclotron frequency.

In both the conical-point and the band-edge scenarios, one possible way to explain the drop in resistivity reported in Refs. [55,56] is to attribute it to a crystallizationlike first-order transition, which leads to the emergence of the spin superstructure and is accompanied by a sudden increase of the mean free path of quasiparticle excitations. This would be similar to what occurs with simple metals as they undergo a first-order crystallization transition. In the framework of the conical-point scenario, the possibility of the resistivity drop is further strengthened by the fact that, like in graphene, a Fermi surface reduced to a few conical points suppresses the scattering of the quasiparticles and hence should significantly increase their mobility. The alternative interpretation is the one proposed by the authors of Ref. [55] and supported by the strong magnetic-field dependence of the resistivity drop, namely, that it is caused by the onset of two-dimensional fluctuating superconductivity. This interpretation as such does not discriminate between stripes and checkerboards. Superconductivity in the presence of stripes was considered in Ref. [57], while, for the spin-vortex checkerboard, it was done in Ref. [58].

The multitude of bands arising for the spin-vortex checkerboard and their dependence on the model parameters prevent us from making definite predictions about the Seebeck coefficient. If, however, our assumption that the minimization of the total energy of the system requires the modulation parameters to adjust themselves in such a way that the chemical potential becomes pinned at the bottom of the pseudogap is correct, then the density of states should be nearly symmetric with respect to the chemical potential, which, in turn, would suggest that the Seebeck coefficient is close to zero and can easily change sign as a function of temperature or doping. Such a behavior of the Seebeck coefficient is indeed observed experimentally (see Ref. [29]).

Finally, we remark that one of the likely features of spin-vortex checkerboard modulations irrespective of a particular scenario is that *more than one band* comes close to the Fermi surface. It is therefore to be expected that such features are to be seen by ARPES. This proposition is consistent with the ARPES experiment in Ref. [15] reporting the observation of two bands for a particular momentum cut through the BZ.

VII. CONCLUSIONS

We calculated the band structure for the model of noninteracting fermions in the background of a spin-vortex checkerboard and analyzed the symmetry properties and degeneracies of the resulting bands. We have proven that each band is doubly degenerate and has at least one conical point where it touches another doubly degenerate band. We then considered two scenarios for the emergence of the pseudogap: (i) the conical-point scenario and (ii) the band-edge scenario. For the model parameters estimated to be relevant to 1/8-doped lanthanum cuprates, the isolated conical-point scenario is not realizable because the Fermi surfaces corresponding to the energies of each of the available conical points also contain additional regular pockets. The conical feature is, nevertheless, robust because it is symmetry protected. Therefore, the conical-point scenario may become relevant if the model Hamiltonian is further generalized to include terms representing charge modulations and superconducting fluctuations. As for the band-edge scenario, we performed a concrete calculation, which led to the Fermi surface containing Fermi arcs along the nodal directions, in agreement with experiments, and some low-intensity spots not observed experimentally. Our analysis

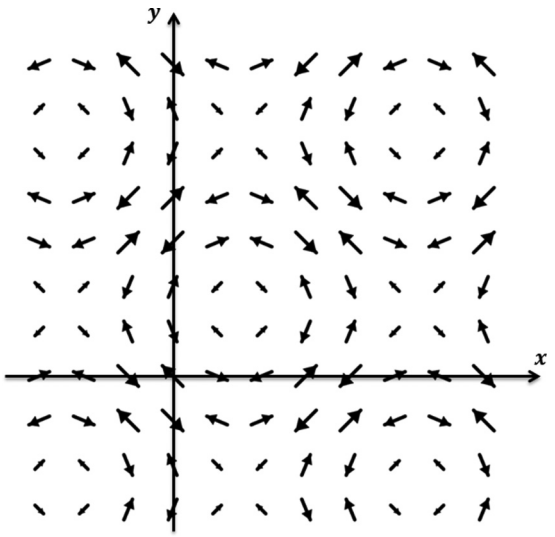

FIG. 8. Plaquette-centered checkerboard corresponding to $\phi_1 = \phi_2 = \pi/8$ in Eq. (3).

indicates that quantum oscillations of transport coefficients would be suppressed in the presence of a spin-vortex checkerboard within either of the above scenarios. It also appears that our model is largely consistent with the measurements of the resistivity and Seebeck coefficient in 1/8-doped lanthanum cuprates.

ACKNOWLEDGMENTS

We would like to thank G. A. Starkov and A. A. Katanin for discussions. This work was supported by Skoltech NGP Program (Skoltech-MIT joint project).

APPENDIX A: FOUR TIMES DEGENERACY AT $\mathbf{k_0} = (\frac{\pi}{8}, \frac{\pi}{8})$

Let us consider one fermion on the spin-vortex checkerboard lattice and parametrize its wave function as follows:

$$\psi(x,y) = u(x,y)\begin{pmatrix}1\\0\end{pmatrix} + v(x,y)\begin{pmatrix}0\\1\end{pmatrix}, \tag{A1}$$

where $u(x,y)$ and $v(x,y)$ are spatial functions defined on the two-dimensional lattice plane and $\binom{1}{0}$ and $\binom{0}{1}$ correspond to spin projections on the z axis. For convenience, we also introduce the operator

$$\hat{T}_{xy} \equiv i\hat{T}_x\hat{T}_y = \hat{\tau}_{(4,4)} \otimes \sigma_z, \tag{A2}$$

representing translation by vector (4,4) with subsequent rotation of spins through 180° about the z axis.

Let us recall that the time-reversal operator $\mathcal{T}$ acts on a wave function given by Eq. (A1) as follows:

$$\mathcal{T}\psi = iu^*(x,y)\begin{pmatrix}0\\1\end{pmatrix} - iv^*(x,y)\begin{pmatrix}1\\0\end{pmatrix}. \tag{A3}$$

Note that $\mathcal{T}^2 = -1$. The important property of the time-reversal operator is that it reverses both the spin and the wave vector. Another useful property is the anticommutation relation $\{\hat{\tau}_{x,y}\mathcal{T}, \hat{T}_{x,y}\} = 0$.

From now on, we focus our attention on functions $u(x,y)$ and $v(x,y)$, which correspond to $\mathbf{k}_0 = (\frac{\pi}{8}, \frac{\pi}{8})$. From Bloch's theorem, it follows that such functions are antiperiodic with respect to translation by eight lattice constants, i.e., $u(x+8,y) = u(x,y+8) = -u(x,y)$. Note that, for such wave functions, $\hat{T}_x^2 = \hat{T}_y^2 = \hat{T}_{x,y}^2 = 1$. By analogy with spin operators, we introduce operators $\hat{Q} = \hat{T}_x + i\hat{T}_y$, $\hat{Q}^\dagger = \hat{T}_x - i\hat{T}_y$, which can be considered as raising and lowering operators while acting on eigenstates of operator $\hat{T}_{x,y}$:

$$[\hat{T}_{x,y}, \hat{Q}^{(\dagger)}] = \mp 2\hat{Q}^{(\dagger)}. \tag{A4}$$

Since each energy level is doubly degenerate, it is convenient to characterize each eigenstate by two quantum numbers: the energy and eigenvalue λ of the operator $\hat{T}_{x,y}$, which can take values ± 1.

Let us consider an energy eigenstate ψ with $\lambda = 1$, i.e., $\hat{T}_{x,y}\psi = \psi$. From ψ we can construct a new state $\tilde{\psi} = \hat{\tau}_{x,y}\mathcal{T} \circ \hat{Q}\psi$, which has the same energy and the same $\lambda = 1$. The fact that $\tilde{\psi}$ has the same $\lambda = 1$ follows from the fact that the operator $\hat{Q}$ lowers λ to -1, but since operators $\hat{\tau}_{x,y}\mathcal{T}$ and $\hat{T}_{x,y}$ anticommute, $\hat{\tau}_{x,y}\mathcal{T}$ raises λ back to 1. Our goal now is to show that ψ and $\tilde{\psi}$ are two linearly independent states. This, together with our previous argument for the twofold degeneracy of each energy band, will prove the desired fourfold degeneracy.

Using the definition of the operator $\hat{Q}$, one can check that

$$\begin{aligned}\psi_1 = \hat{Q}\psi &= i(\hat{\tau}_{4x}u - \hat{\tau}_{4y}u)\begin{pmatrix}0\\1\end{pmatrix} + i(\hat{\tau}_{4x}v + \hat{\tau}_{4y}v)\begin{pmatrix}1\\0\end{pmatrix}\\ &= 2i\hat{\tau}_{4x}u\begin{pmatrix}0\\1\end{pmatrix} + 2i\hat{\tau}_{4x}v\begin{pmatrix}1\\0\end{pmatrix},\end{aligned} \tag{A5}$$

where, in the last equality, we imply that $\hat{\tau}_{x,y}u = u$ and $\hat{\tau}_{x,y}v = -v$, which follow from $\hat{T}_{x,y}\psi = \psi$. Using Eq. (A3), we then obtain

$$\tilde{\psi} = \hat{\tau}_{x,y}\mathcal{T}\psi_1 = -2(\hat{\tau}_{4x}u)^*\begin{pmatrix}1\\0\end{pmatrix} - 2(\hat{\tau}_{4x}v)^*\begin{pmatrix}0\\1\end{pmatrix}. \tag{A6}$$

Therefore, ψ and $\tilde{\psi}$ are linearly dependent if and only if

$$u^* = \alpha\hat{\tau}_{4x}u, \tag{A7}$$

$$v^* = \alpha\hat{\tau}_{4x}v, \tag{A8}$$

where α is some nonzero complex number. We can use the last two equations to obtain

$$\begin{aligned}u(x,y) = (u^*)^* &= [\alpha u(x+4,y)]^* = \alpha^* u^*(x+4,y)\\ &= |\alpha|^2 u(x+8,y) = -|\alpha|^2 u(x,y).\end{aligned} \tag{A9}$$

The same relation holds for v. For nonzero $u(x,y)$ and $v(x,y)$, the two relations can be satisfied only when $\alpha = 0$, which means that ψ and $\tilde{\psi}$ are linearly independent. This completes the proof of the fourfold degeneracy of each energy level at $\mathbf{k}_0 = (\frac{\pi}{8}, \frac{\pi}{8})$.

APPENDIX B: EIGHTFOLD DEGENERACY AT $\mathbf{k_0} = (\frac{\pi}{8}, \frac{\pi}{8})$ FOR THE PLAQUETTE-CENTERED CHECKERBOARD

Let us introduce three more symmetry transformations specific to the case of the plaquette-centered

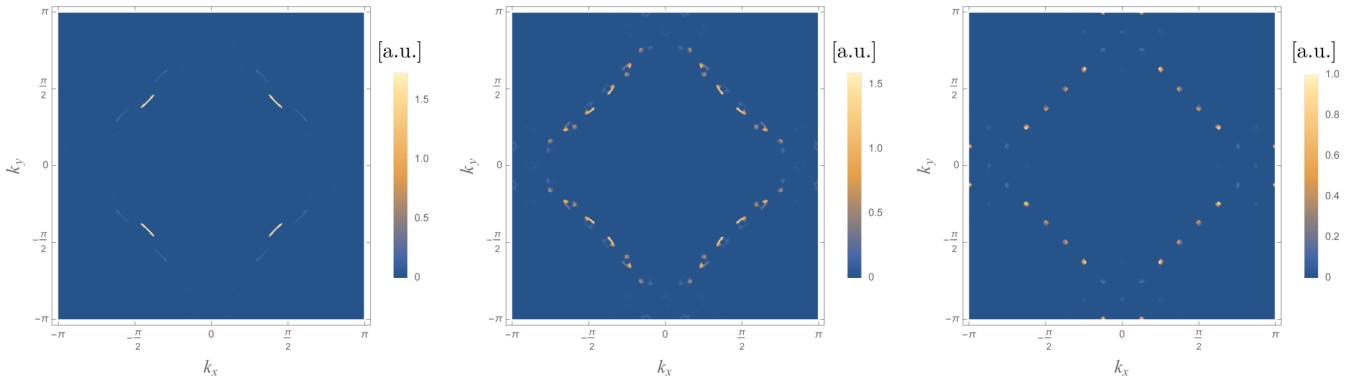

FIG. 9. Mapping of the Fermi-surface pockets from the small BZ shown in Fig. 3 to the large BZ: (a) the largest pocket (red dashed line in Fig. 3), (b) the intermediate pocket (blue dashed line in Fig. 3), and (c) the smallest pocket (blue solid line in Fig. 3).

checkerboard:

$$\hat{A}_x \equiv R_x \hat{\tau}_{(0,1)} \otimes \sigma_z, \tag{B1}$$

$$\hat{A}_y \equiv R_y \hat{\tau}_{(1,0)} \otimes \sigma_z, \tag{B2}$$

$$\hat{S} \equiv \hat{A}_x \hat{A}_y = \hat{I} \hat{\tau}_{(1,1)}, \tag{B3}$$

where R_x (R_y) denotes spatial reflection with respect to the x axis (y axis) shown in Fig. 8 and $\hat{I}$ denotes the spatial inversion with respect to the coordinate origin shown in Fig. 8. All three operators, $\hat{A}_x$, $\hat{A}_y$, and $\hat{S}$, commute with each other and with the Hamiltonian $\mathcal{H}$.

Operators $\hat{A}_x$ and $\hat{A}_y$ anticommute with $\hat{T}_{x,y}$. In order to show this, let us consider some function $f(x,y)$ that has spatial periodicity corresponding to $\mathbf{k}_0 = (\frac{\pi}{8}, \frac{\pi}{8})$. In this case, we find

$$\begin{aligned} R_x \hat{\tau}_{(0,1)} \hat{\tau}_{(4,4)} f(x,y) &= f(x+4,-y-5), \\ \hat{\tau}_{(4,4)} R_x \hat{\tau}_{(0,1)} f(x,y) &= f(x+4,-y+3) \\ &= -f(x+4,-y-5), \end{aligned}$$

which implies that $\hat{S}$ commutes with $\hat{T}_{x,y}$, because the operator $\hat{S}$ is a product of operators $\hat{A}_x$ and $\hat{A}_y$, each of which anticommutes with $\hat{T}_{x,y}$. As a result, each eigenstate can be characterized, in addition to λ, by a quantum number λ_s associated with the operator $\hat{S}$.

Consider state ψ with $\lambda = 1, \lambda_s = 1$. We now observe that $\tilde{\psi} = \hat{\tau}_{x,y} \mathcal{T} \hat{A}_x \psi$ is a state with the same energy and with $\lambda = 1, \lambda_s = 1$. Indeed, both operators $\hat{\tau}_{x,y}\mathcal{T}$ and $\hat{A}_x$ anticommute with $\hat{T}_{x,y}$, so that their product commutes with $\hat{T}_{x,y}$; both of them as well as their product commute with $\hat{S}$.

Let us write $\tilde{\psi}$ explicitly,

$$\tilde{\psi} = i u^*(x,-y-1) \begin{pmatrix} 0 \\ 1 \end{pmatrix} - i v^*(x,-y-1) \begin{pmatrix} 1 \\ 0 \end{pmatrix}, \tag{B4}$$

and then prove that $\tilde{\psi}$ and ψ [given by Eq. (A1)] are linearly independent. They are linearly dependent if and only if

$$u(x,y) = -\alpha v^*(x,-y-1), \tag{B5}$$

$$v(x,y) = \alpha u^*(x,-y-1) \tag{B6}$$

for some nonzero complex number α. We can use the last two equations to obtain

$$u(x,y) = -|\alpha|^2 u(x,y). \tag{B7}$$

The same identity holds for $v(x,y)$. For nonzero $u(x,y)$ and $v(x,y)$, the last identity can be satisfied only when $\alpha = 0$, but this means the linear independence of ψ and $\tilde{\psi}$. From this, it follows that point $\mathbf{k}_0 = (\frac{\pi}{8}, \frac{\pi}{8})$ for the plaquette-centered case has an additional twofold degeneracy, which, together with the previously proven general fourfold degeneracy, implies the overall eightfold degeneracy.

APPENDIX C: MAPPING INDIVIDUAL FERMI-SURFACE POCKETS TO THE LARGE BZ

In Fig. 9, we present the individual mapping of each of the three small-BZ Fermi-surface pockets shown in Fig. 3 to the large BZ. Figure 9 supplements the discussion in Sec. V C.

[1] J. M. Tranquada, B. J. Sternlieb, J. D. Axe, Y. Nakamura, and S. Uchida, Nature (London) **375**, 561 (1995).

[2] K. Yamada, C. H. Lee, K. Kurahashi, J. Wada, S. Wakimoto, S. Ueki, H. Kimura, Y. Endoh, S. Hosoya, G. Shirane *et al.*, Phys. Rev. B **57**, 6165 (1998).

[3] J. E. Hoffman, E. W. Hudson, K. M. Lang, V. Madhavan, H. Eisaki, S. Uchida, and J. C. Davis, Science **295**, 466 (2002).

[4] K. McElroy, R. W. Simmonds, J. E. Hoffman, D.-H. Lee, J. Orenstein, H. Eisaki, S. Uchida, and J. C. Davis, Nature (London) **422**, 592 (2003).

[5] M. Vershinin, S. Misra, S. Ono, Y. Abe, Y. Ando, and A. Yazdani, Science **303**, 1995 (2004).

[6] T. Hanaguri, C. Lupien, Y. Kohsaka, D.-H. Lee, M. Azuma, M. Takano, H. Takagi, and J. C. Davis, Nature (London) **430**, 1001 (2004).

[7] P. Abbamonte, A. Rusydi, S. Smadici, G. D. Gu, G. A. Sawatzky, and D. L. Feng, Nat. Phys. **1**, 155 (2005).

[8] K. McElroy, D.-H. Lee, J. E. Hoffman, K. M. Lang, J. Lee, E. W. Hudson, H. Eisaki, S. Uchida, and J. C. Davis, Phys. Rev. Lett. **94**, 197005 (2005).

[9] W. D. Wise, M. C. Boyer, K. Chatterjee, T. Kondo, T. Takeuchi, H. Ikuta, Y. Wang, and E. W. Hudson, Nat. Phys. **4**, 696 (2008).

[10] E. H. da Silva Neto, P. Aynajian, A. Frano, R. Comin, E. Schierle, E. Weschke *et al.*, Science **343**, 393 (2014).

[11] R. Comin, R. Sutarto, F. He, E. H. da Silva Neto, L. Chauviere *et al.*, Nat. Mater. **14**, 796 (2015).

[12] T. Valla, A. V. Fedorov, J. Lee, J. C. Davis, and G. D. Gu, Science **314**, 1914 (2006).

[13] R.-H. He, K. Tanaka, S.-K. Mo, T. Sasagawa, M. Fujita, T. Adachi, N. Mannella, K. Yamada, Y. Koike, Z. Hussain, and Z.-X. Shen, Nat. Phys. **5**, 119 (2009).

[14] C. E. Matt, C. G. Fatuzzo, Y. Sassa, M. Månsson, S. Fatale, V. Bitetta, X. Shi, S. Pailhès, M. H. Berntsen, T. Kurosawa *et al.*, Phys. Rev. B **92**, 134524 (2015).

[15] J. Chang, Y. Sassa, S. Guerrero, M. Månsson, M. Shi, S. Pailhes, A. Bendounan, R. Mottl, T. Claesson, O. Tjernberg *et al.*, New J. Phys. **10**, 103016 (2008).

[16] N. Barišić, S. Badoux, M. K. Chan, C. Dorow, W. Tabis, B. Vignolle, G. Yu, J. Béard, X. Zhao, C. Proust, and M. Greven, Nat. Phys. **9**, 761 (2013).

[17] N. Doiron-Leyraud, S. Badoux, S. René de Cotret, S. Lepault, D. LeBoeuf, F. Laliberté *et al.*, Nat. Commun. **6**, 6034 (2015).

[18] N. Doiron-Leyraud, C. Proust, D. LeBoeuf, J. Levallois, J.-B. Bonnemaison, R. Liang, D. A. Bonn, W. N. Hardy, and L. Taillefer, Nature (London) **447**, 565 (2007).

[19] S. E. Sebastian, N. Harrison, R. Liang, D. A. Bonn, W. N. Hardy, C. H. Mielke, and G. G. Lonzarich, Phys. Rev. Lett. **108**, 196403 (2012).

[20] S. E. Sebastian, N. Harrison, C. H. Mielke, R. Liang, D. A. Bonn, W. N. Hardy, and G. G. Lonzarich, Phys. Rev. Lett. **103**, 256405 (2009).

[21] B. Vignolle, A. Carrington, R. A. Cooper, M. M. J. French, A. P. Mackenzie, C. Jaudet, D. Vignolles, Cyril Proust, and N. E. Hussey, Nature (London) **455**, 952 (2008).

[22] A. J. Millis and M. R. Norman, Phys. Rev. B **76**, 220503 (2007).

[23] S. Chakravarty and H.-Y. Kee, Proc. Natl Acad. Sci. USA **105**, 8835 (2008).

[24] W.-Q. Chen, K.-Y. Yang, T. M. Rice, and F. C. Zhang, Europhys. Lett. **82**, 17004 (2008).

[25] V. B. Zabolotnyy, A. A. Kordyuk, D. S. Inosov, D. V. Evtushinsky, R. Schuster, B. Büchner, N. Wizent, G. Behr, S. Pyon, and T. Takayama, Europhys. Lett. **86**, 47005 (2009).

[26] H. Yao, D.-H. Lee, and S. Kivelson, Phys. Rev. B **84**, 012507 (2011).

[27] N. Harrison and S. E. Sebastian, Phys. Rev. Lett. **106**, 226402 (2011).

[28] A. Allais, D. Chowdhury, and S. Sachdev, Nat. Commun. **5**, 5771 (2014).

[29] F. Laliberte, J. Chang, N. Doiron-Leyraud, E. Hassinger, R. Daou *et al.*, Nat. Commun. **2**, 432 (2011).

[30] N. B. Christensen, H. M. Rønnow, J. Mesot, R. A. Ewings, N. Momono, M. Oda, M. Ido, M. Enderle, D. F. McMorrow, and A. T. Boothroyd, Phys. Rev. Lett. **98**, 197003 (2007).

[31] B. V. Fine, Phys. Rev. B **70**, 224508 (2004).

[32] B. V. Fine, Phys. Rev. B **75**, 014205 (2007).

[33] B. V. Fine, Phys. Rev. B **75**, 060504 (2007).

[34] B. V. Fine, J. Supercond. Novel Magn. **24**, 1207 (2011).

[35] J. G. Brandenburg and B. V. Fine, J. Supercond. Novel Magn. **26**, 2621 (2013).

[36] S. A. Kivelson, I. P. Bindloss, E. Fradkin, V. Oganesyan, J. M. Tranquada, A. Kapitulnik, and C. Howald, Rev. Mod. Phys. **75**, 1201 (2003).

[37] J. A. Robertson, S. A. Kivelson, E. Fradkin, A. C. Fang, and A. Kapitulnik, Phys. Rev. B **74**, 134507 (2006).

[38] J. Zaanen and O. Gunnarsson, Phys. Rev. B **40**, 7391 (1989).

[39] G. Seibold, R. S. Markiewicz, and J. Lorenzana, Phys. Rev. B **83**, 205108 (2011).

[40] J. M. Tranquada, in *Handbook of High-Temperature Superconductivity*, edited by J. R. Schrieffer and J. S. Brooks (Springer, Berlin, 2006), pp. 257–298.

[41] R. Comin, R. Sutarto, E. H. da Silva Neto, L. Chauviere, R. Liang, W. N. Hardy, D. A. Bonn, F. He, G. A. Sawatzky, and A. Damascelli, Science **347**, 1335 (2015).

[42] B. V. Fine, Science **351**, 235 (2016).

[43] R. Comin, R. Sutarto, E. H. da Silva Neto, L. Chauviere, R. Liang, W. N. Hardy, D. A. Bonn, F. He, G. A. Sawatzky, and A. Damascelli, Science **351**, 235 (2016).

[44] Y. Wang and A. V. Chubukov, Phys. Rev. B **92**, 245140 (2015).

[45] H. Jang, W.-S. Leeb, H. Nojiric, S. Matsuzawac, H. Yasumurac *et al.*, Proc. Natl. Acad. Sci. USA **113**, 14645 (2016).

[46] S. Avci, O. Chmaissem, S. Rosenkranz, J. M. Allred, I. Eremin, A. V. Chubukov *et al.*, Nat. Commun. **5**, 3845 (2014).

[47] A. E. Böhmer, F. Hardy, L. Wang, T. Wolf, P. Schweiss, and C. Meingast, Nat. Commun. **6**, 7911 (2015).

[48] J. O'Halloran, D. F. Agterberg, M. X. Chen, and M. Weinert, Phys. Rev. B **95**, 075104 (2017).

[49] W. R. Meier, Q.-P. Ding, A. Kreyssig, S. L. Bud'ko, A. Sapkota *et al.*, arXiv:1706.01067.

[50] A. K. Geim and K. S. Novoselov, Nat. Mater. **6**, 183 (2007).

[51] E. Pavarini, I. Dasgupta, T. Saha-Dasgupta, O. Jepsen, and O. K. Andersen, Phys. Rev. Lett. **87**, 047003 (2001).

[52] K. M. Kojima, H. Eisakia, S. Uchida, Y. Fudamoto, I. M. Gat, A. Kinkhabwala, M. I. Larkin, G. M. Luke, and Y. J. Uemura, Physica B (Amsterdam, Neth.) **289-290**, 343 (2000).

[53] T. Egami, B. V. Fine, D. Parshall, A. Subedi, and D. J. Singh, Adv. Condens. Matter. Phys. **2010**, 164916 (2010).

[54] N. W. Ashcroft and N. D. Mermin, *Solid State Physics* (Saunders College, Philadelphia, 1976).

[55] Q. Li, M. Hücker, G. D. Gu, A. M. Tsvelik, and J. M. Tranquada, Phys. Rev. Lett. **99**, 067001 (2007).

[56] J. M. Tranquada, G. D. Gu, M. Hücker, Q. Jie, H.-J. Kang *et al.*, Phys. Rev. B **78**, 174529 (2008).

[57] E. Berg, E. Fradkin, E.-A. Kim, S. A. Kivelson, V. Oganesyan, J. M. Tranquada, and S. C. Zhang, Phys. Rev. Lett. **99**, 127003 (2007).

[58] V. Bhartiya and B. V. Fine, arXiv:1703.09979.